Altered levels of the splicing factor muscleblind modifies cerebral cortical function in mouse models of myotonic dystrophy

Gang Chen[a], **Russell E. Carter**[a], **John D. Cleary**[b], **Tammy S. Reid**[b], **Laura P. Ranum**[b], **Maurice S. Swanson**[b], **Timothy J. Ebner**[a],[*]

[a]Department of Neuroscience, University of Minnesota, Minneapolis, MN, USA

[b]Center for NeuroGenetics, Department of Molecular Genetics & Microbiology and Neurology, College of Medicine, Genetics Institute, University of Florida, Gainesville, FL, USA

Abstract

Myotonic dystrophy (DM) is a progressive, multisystem disorder affecting skeletal muscle, heart, and central nervous system. In both DM1 and DM2, microsatellite expansions of CUG and CCUG RNA repeats, respectively, accumulate and disrupt functions of alternative splicing factors, including muscleblind (MBNL) proteins. Grey matter loss and white matter changes, including the corpus callosum, likely underlie cognitive and executive function deficits in DM patients. However, little is known how cerebral cortical circuitry changes in DM. Here, flavoprotein optical imaging was used to assess local and contralateral responses to intracortical motor cortex stimulation in DM-related mouse models. In control mice, brief train stimulation generated ipsilateral and contralateral homotopic fluorescence increases, the latter mediated by the corpus callosum. Single pulse stimulation produced an excitatory response with an inhibitory-like surround response mediated by $GABA_A$ receptors. In a mouse model of DM2 (*Mbnl2* KO), we observed prolonged and increased responsiveness to train stimulation and loss of the inhibition from single pulse stimulation. Conversely, mice overexpressing human MBNL1 (MBNL1-OE) exhibited decreased contralateral response to train stimulation and reduction of inhibitory-like surround to single pulse stimulation. Therefore, altering levels of two key DM-associated splicing factors modifies functions of local cortical circuits and contralateral responses mediated through the corpus callosum.

Keywords

Corpus callosum; flavoprotein; MBNL; Microsatellite repeats; Myotonic dystrophy

[*]Corresponding author at: Department of Neuroscience, University of Minnesota, Lions Research Building Room 421, 2001 Sixth Street SE, Minneapolis, MN 55455, USA., ebner001@umn.edu (T.J. Ebner).

Conflicts of interest
None.

1. Introduction

Myotonic dystrophy (DM) types 1 and 2 are adult-onset, autosomal dominant, progressive multisystem disorders (Harper 2001). DM1 and DM2 are clinically similar disorders with patients developing muscle wasting and myotonia, cardiac arrhythmias, iridescent cataracts, and central nervous system (CNS) abnormalities. Both DM1 and DM2 result from microsatellite repeat expansions in functionally distinct genes. DM1 is caused by a CTG expansion in the 3′ UTR of the *dystrophia myotonica protein kinase* (*DMPK*) gene and DM2 from an intronic CCTG expansion in the *CCHC-type zinc finger, nucleic acid binding protein* (*CNBP*) gene (Brook et al. 1992;Mahadevan et al. 1992;Fu et al. 1992;Liquori et al. 2001).

There is substantial support that DM1 CUG and DM2 CCUG expansion transcripts accumulate in RNA foci and disrupt alternative splicing factors, including the MBNL and CUG-BP- and ETR-3-like factors (CELF) proteins. Mouse models that demonstrate missplicing and/ or loss of MBNL proteins reproduce many of the systemic and CNS splicing abnormalities (Gomes-Pereira et al. 2007;Du et al. 2010;Charizanis et al. 2012;Suenaga et al. 2012;Hernandez-Hernandez et al. 2013). The sequestration of splicing factors by repeat expansion RNA transcripts not only provides for a compelling model of disease pathogenesis but also a potential therapeutic approach to DM based on upregulation of members of the MBNL family (Chamberlain and Ranum 2012).

Patients with either type of DM have debilitating neurological dysfunction including cognitive deficits (Harper 2001). The cognitive deficits in DM patients include visual-spatial abnormalities, attention deficits, and impaired executive functioning (Rubinsztein et al. 1997;Meola et al. 2003;Modoni et al. 2004;Minnerop et al. 2011). While DM1 patients are more likely to exhibit greater deficits than DM2 patients, the latter can have similar cognitive impairments (van Spaendonck et al. 1995;Meola et al. 1999;Meola et al. 2003;Gaul et al. 2006). Anatomical and diffusion tensor imaging (DTI) documents widespread changes in the cerebral cortical white matter in DM1 and DM2 patients including in the corpus callosum (Fukuda et al. 2005;Ota et al. 2006;Wozniak et al. 2011;Minnerop et al. 2011;Franc et al. 2012). Gray matter cell loss has also been reported, although less so in DM2 than DM1 patients (Ono et al. 1996;Kassubek et al. 2003;Antonini et al. 2004;Minnerop et al. 2011). Furthermore, resting state fMRI studies in DM1 patients report changes in resting state connectivity (Serra et al. 2014;Serra et al. 2016). These findings suggest that cerebral cortical circuits are altered in DM, particularly white matter tracts (Minnerop et al. 2011).

The abnormalities in white matter integrity, loss of grey matter, and changes in functional connectivity are hypothesized to contribute to the CNS deficits in DM patients (Antonini et al. 2004;Wozniak et al. 2011;Minnerop et al. 2011;Franc et al. 2012). However, little is known whether DM mouse models have comparable alterations in the cerebral cortical circuitry. To begin to address this issue, we developed a flavoprotein-based optical imaging assay of the effects of intracortical stimulation to map both local response as well as the response to activation of the corpus callosum (Shibuki et al. 2003;Reinert et al. 2004;Reinert et al. 2007). Flavoprotein autofluorescence is an activity-dependent signal based on

changes in neuronal oxidation metabolism (Chance 1991;Shibuki et al. 2003;Reinert et al. 2004;Reinert et al. 2011). The flavoprotein signal reflects the underlying neuronal responses as assessed by field potentials or single unit activity and is therefore, a highly useful mapping signal (Shibuki et al. 2003;Coutinho et al. 2004;Husson et al. 2007;Wang et al. 2011;Cramer et al. 2013). Flavoprotein imaging, like intrinsic optical imaging (Lieke et al. 1989), allows for a wide field-of-view of neuronal activity across a large area of the brain (Cramer et al. 2015;Ma et al. 2016;Kozberg et al. 2016). Therefore, this type of mesoscopic imaging provides an important tool to evaluate normal and abnormal response patterns and complements the cellular resolution, but more limited field-of-view, of two-photon imaging.

Next, we used this assay to investigate two mouse models related to DM. The first model is a *Mbnl2* knockout (*Mbnl2*$^{(\Delta E2/\Delta E2)}$) that develops many of the features of DM including deficits in synaptic transmission and plasticity (Charizanis et al. 2012). Importantly, MBNL2 is the principal splicing factor disrupted in the CNS, and *Mbnl2* KO mice do not develop muscle deficits. The second model involves two lines of transgenic mice that overexpress human MBNL1 (MBNL1-OE) in the CNS that were developed to test the therapeutic possibility of reversing the effect of sequestration of MBNL proteins by microsatellite expansions (Chamberlain and Ranum 2012).

2. Materials and Methods

2.1. Transgenic mice

To establish the normal responses to intracortical stimulation, male FVB mice, ages 4–8 months (Charles River Laboratories, Wilmington) were used. As described in the original publication (Chamberlain and Ranum 2012), L14686 mice overexpressing a 40 kDa isoform of human MBNL1 were generated on the FVB background using the β-actin promotor. In addition to the previously published L14686 line (Chamberlain and Ranum 2012) we generated and examined a second independent transgenic mouse line (L15132) that overexpresses the same 40 kDa MBNL1 isoform in the CNS. This line, which constitutively overexpresses MBNL1, was generated from a construct expressing the same N-terminal FLAG-tagged humanized version of MBNL1 in which a floxed stop cassette had been removed by crosses with the Ella-Cre transgenic line (JAX Lab # 003314). This recombination event had been stably transmitted to the F2 progeny. The resulting singly transgenic MBNL1 positive progeny constitutively express the FLAG-tagged MBNL1 from early embryogenesis. The expression level of MBNL1 in this newly developed line (L15132) and that of the L14686 line was confirmed by immunoblot analyses. MBNL1 overexpression in both lines is generally well tolerated and has been previously described in detail for the L14686 line (Chamberlain and Ranum 2012). The generation and characterization of the *Mbnl2* KO mice was previously described (Charizanis et al. 2012), and used a homologous recombination strategy in which *Mbnl2* exon 2 was deleted, as this exon encodes the initiation codon for the full length MBNL2 protein (Kanadia et al. 2003). The resultant *Mbnl2*$^{(\Delta E2/\Delta E2)}$ mice (referred to as *Mbnl2* KO mice) were on a C57Bl/6 background.

2.2. Animal preparation

All animal procedures were approved by and conducted in conformity with the Institutional Animal Care and Use Committee of the University of Minnesota and the University of Florida and in accordance with the National Institutes of Health guide for the care and use of Laboratory animals (NIH Publications No. 8023, revised 1978). For physiological studies in the normal or the DM-related mice, the animals were anesthetized by an initial intramuscular injection of 2.0 mg/kg acepromazine followed by an intraperitoneal injection of 1.2 mg/kg urethane and supplemented with 0.3 mg/kg urethane as needed. The electrocardiogram and response to toe pinch were monitored to assess the depth of anesthesia. The mice were placed in a stereotaxic frame, mechanically ventilated and body temperature feedback-regulated. A large craniotomy was performed bilaterally over the cerebral cortex that included the motor cortical areas, and the dura carefully removed. A watertight dental acrylic chamber was created around the exposed cortex and was filled and frequently rinsed with warmed (37 °C) Ringer's solution gassed with 95% O_2/5% CO_2.

2.3. Optical imaging

Images were acquired with a high-speed, cooled charged-coupled device (CCD) macroscope (Nikon AZ-100) with a 512×512 chip using a 2× objective. Images were binned at 256×256 pixels, resulting in a pixel resolution of ~28×28 μm (MetaMorph, Sunnyvale, CA). The camera was focused 200–300 μm below the cerebral cortical surface. Flavoprotein autofluorescence imaging used a band-pass excitation filter (455 ± 35 nm), an extended reflectance dichroic mirror (500 nm), and a>515 nm long-pass emission filter (Reinert et al. 2004). Responses are reported as F/F_0 (%), with F_0 being the average of the first 20 pre-stimulation frames of an image series consisting of 80 sequential frames (200 ms per frame) for single pulse stimulations or 425 sequential frames (200 ms per frame) for train stimulation (see below).

2.4. Direct cortical stimulation

Direct electrical stimulation of the motor cortex was delivered by a parylene coated microelectrode (2–5MΩ) placed ~300–400 μm below the surface of the motor cortex (~1.5mm rostral and lateral to bregma). In several preliminary experiments, these coordinates were found to evoke strong and consistent ipsilateral and contralateral optical responses. Three stimulation protocols were used. The first protocol (used in Figs. 1, 2, 5, 6, and 8) consisted of a one second train of 10 pulses (200 μA, 100 μs) at 10 Hz to establish the ipsilateral and contralateral response patterns in both wild-type mice and DM models. Typically, this stimulus train was repeated 4–6 times at an interval of 5 min to establish the baseline responses in wild-type and disease models. In animals with a pharmacological manipulation, the baseline stimulation was followed by up to 4 repetitions after application of a drug. The second protocol (used in Fig. 3) was designed to map the optical responses with field potential recordings and consisted of a single pulse (100 μs, 100 μA), repeated 16 times at 1 s intervals. The field potential responses evoked by the 16 stimuli were averaged. The third stimulation protocol used a single pulse stimulation to investigate whether intracortical stimulation evoked an inhibitory component, as the expected inhibitory-like surround was not evident with the first two stimulation protocols. In

this third protocol (used in Figs. 4, 7, and 9), a single pulse (200 μA, 100 μs) was repeated 16 times at 20 s intervals, averaging the results from the 16 stimuli. This block of averaged 16 stimulations was repeated 4–6 times to establish the responses for wild-type or DM mice as well as prior to and after drug application.

2.5. Analysis of the optical responses

To quantify changes in the flavoprotein autofluorescence responses to direct electrical stimulation, regions of interest (ROIs) were defined visually. The ROIs were circular (0.8mm diameter) and were placed over the center of the ipsilateral and contralateral regions of increased fluorescence for the 10 Hz train stimulation protocols (see Fig. 1). The train stimulation evoked an initial increase in fluorescence followed by a decrease in fluorescence (Shibuki et al. 2003;Reinert et al. 2004;Coutinho et al. 2004;Cramer et al. 2015). The former results from the oxidation of mitochondrial flavoproteins in postsynaptic neurons and is tightly coupled to stimulation strength (Shibuki et al. 2003;Reinert et al. 2004;Brennan et al. 2006;Reinert et al. 2007). All analyses of the responses to the train stimulation were based on the increase in fluorescence. To quantify the amplitude of the response to train stimulation in the selected ROI, we determined the average F/F_0 for the five frames centered on the peak increase in fluorescence. The single pulse stimulation evoked a more complex response consisting of a central region with an increase in fluorescence surrounded by a region of decreased fluorescence. Therefore, the analyses of the responses included placing the circular ROIs over the center of the ipsilateral and contralateral regions of increased fluorescence, and in the surrounding regions of decreased fluorescence (see Fig. 4A). The placement of the ROIs was chosen based on visual observation to obtain the maximal (center) or minimal (surround) flavoprotein response to stimulation. Therefore, between animals, the ROI placement will differ depending on the location of the maximal and minimum responses. However, within the same animal, ROI placement remained constant throughout baseline and drug application. The response amplitude was measured at two time points: an early time point (early phase) that captured the peak decrease in fluorescence in the surround ROI; and a later time point (late phase) that captured the peak increase in fluorescence in the center ROI (see Fig. 4B and C). At both time points, the average F/F_0 over 2 frames (0.4 s) was determined.

2.6. Field potential recordings and analysis

Field potentials were recorded at a depth of 300 μm in the contralateral cortex to intracortical stimulation (16 single pulses with a 1 s interval) using glass microelectrodes filled with 2M NaCl (2–5MΩ), digitized at 25 KHz and the responses to the 16 stimuli averaged. The field potentials were recorded at 0.5mm intervals, lateral to medial, across the extent of the evoked flavoprotein response (see Fig. 3). The amplitude of the initial large negativity was determined and used as a measure of the post-synaptic excitatory response (Hoffmeyer et al. 2007).

2.7. Drugs and administration

Various drugs were applied in normal Ringer's solution to the exposed cerebral surface, including: DNQX (6,7-dinitroquinoxaline-2,3-dione disodium salt); APV (D-(−)-2-amino-5-phosphonopentanoic acid); TTX (octahydro-12-(hydoxymethyl)-2-imino-5,9:7,10a-

dimethano-10a*H*-[1,3] dioxocino [6,5-*d*] pyrimidine-4,7,10,11,12-pentol); Gabazine (SR 95531 hydrobromide, 6-Imino-3-(4-methoxyphenyl)-1(6*H*)-pyridazinebutanoic acid hydrobromide); L-NAME (L-N[G]-Nitroarginine methyl ester); indomethacin (2-{1-[(4-Chlorophenyl) carbonyl]-5-methoxy-2-methyl-1H-indol-3-yl}acetic acid). TTX was either bath applied over the entire cortex or was microinjected into the corpus callosum. Microinjections (100 μM TTX, 15–25 psi for 1–2 s) were delivered through a glass microelectrode connected to a pico-injection system (PLI-100; Medical Systems). The insertion point of the microelectrode was −0.6mm anteroposterior, 0.5mm medial lateral relative to bregma, and advanced a total distance of 3.0mm at an angle of 10° off midline, 38° relative to the horizon. This allowed for targeted injection of TTX into the corpus callosum centered between the evoked ipsilateral and contralateral flavoprotein response. All drugs were purchased from Tocris Bioscience (Ellisville, MO).

3. Statistical analysis

The statistical analysis was performed using SAS software (SAS Institute Cary, NC). The effects of the different drugs or genotype on the optical responses were statistically evaluated by the appropriate ANOVA (repeated measures within or between subject designs, $p < 0.05$) followed by post-hoc testing using the Bonferroni method to control for multiple comparisons. In all experiments, the amplitudes of the ipsilateral and contralateral responses differed. Therefore, analyses focused on testing for differences in the responses evoked on the ipsilateral and contralateral sides separately. In experiments comparing the optical and field potential responses, the amplitude of the optical response was regressed against the initial negativity of the field potential at each recording location, and the coefficient of determination (R^2) and F-statistic was determined. Throughout the text and figures, values are reported as mean+standard deviation (SD) and "n" refers to the number of animals used in an experiment.

4. Results

4.1. Flavoprotein responses to intracortical stimulation

We first characterized the flavoprotein responses evoked by direct electrical stimulation of the primary motor cortex in FVB wild-type mice using 10 Hz stimulation for 1 s. We selected the primary motor cortex to study based on a series of preliminary experiments that showed robust and consistent ipsilateral and contralateral responses to intracortical stimulation. Also, the corpus callosum in the mouse is well-developed in this region of the frontal lobes (Mitchell and Macklis 2005;Chovsepian et al. 2017), and changes in the corpus callosum in the frontal lobes have been reported in DM patients (Fukuda et al. 2005;Ota et al. 2006;Wozniak et al. 2011;Minnerop et al. 2011;Franc et al. 2012). Train stimulation evoked a strong increase in flavoprotein autofluorescence in the ipsilateral hemisphere centered on the stimulating electrode, and a concurrent increase in the contralateral hemisphere in the same homotopic area (Fig. 1A), consistent with transmission through the corpus callosum. Following the initial increase in flavoprotein autofluorescence, there was a prolonged decrease in autofluorescence (Fig. 1B), similar to that previously reported for the cerebellar and cerebral cortex (Shibuki et al. 2003;Reinert et al. 2004;Brennan et

al. 2006;Cramer et al. 2015). The response amplitude was $2.38 \pm 0.87\%$ in the ipsilateral hemisphere, but was significantly smaller in the contralateral side at $1.48 \pm 0.58\%$ (Fig. 1C, $F(1,14)=45.48$, n=15, $p < 0.001$). Therefore, flavoprotein imaging can be a useful tool to map both inter- and intrahemispheric neuronal activation.

Next, we addressed the synaptic circuitry involved in the optical responses. As both intracortical and transcallosal projections terminate in glutamatergic synapses and primarily activate post-synaptic AMPA and NMDA receptors (Keller 1993;Kumar and Huguenard 2001), we tested the contributions of these glutamate receptors to the autofluorescence responses. Co-application of the AMPA receptor antagonist DNQX (100 μM) and the NMDA receptor antagonist APV (250 μM) onto the exposed cortex greatly suppressed the flavoprotein response in both the ipsilateral ($F(3,6)=24.89$, $p < 0.001$, Bonferroni, $p < 0.01$) and contralateral ($F(3,6)=61.84$, $p < 0.001$, n=4, Bonferroni, $p < 0.01$) hemispheres (Fig. 2A and B). Local field potentials (LFPs) were also greatly reduced, with only a small negative deflection remaining that most likely represents the afferent fiber volley in the corpus callosum fibers. Interestingly, DNQX/APV did not completely block either the ipsilateral or contralateral optical responses suggesting that other receptor types may be involved in the synaptic activation and that some of the ipsilateral activation was due to the direct effects of stimulation. Another possible explanation is that there was only a partial block of AMPA/NMDA receptors, however, the concentration of antagonists used here have been shown to obtain a high level of glutamate receptor block (Shlosberg et al. 2006;Haley et al. 2016). Washout of the drugs resulted in a significant increase in the response amplitude (Bonferroni, $p < 0.01$ for both hemispheres). Topical application of tetrodotoxin (TTX, 10 μM), completely blocked the autofluorescence in both hemispheres (Bonferroni, $p < 0.01$) and abolished the remaining fiber volley. These findings show that the optical responses in both hemispheres are activity-dependent, with a large contribution from synaptic activation of ionotropic glutamate receptors.

4.2. Involvement of the corpus callosum in the contralateral response

To test if the contralateral response was mediated by the corpus callosum, we stereotaxically injected a small volume of TTX (~30–35 nL, 100 μM) into the corpus callosum (see Materials and Methods.). As shown for an example experiment and the population results (Fig. 2C and D), TTX significantly reduced the optical response in the contralateral hemisphere ($F(1,3)=37.6$, n=4, $p=0.009$, Fig. 2C and D). Conversely, TTX did not alter the ipsilateral response ($F(1,3)=0.35$, $p=0.5934$), Fig. 2C and D), supporting the hypothesis that the contralateral response is evoked primarily through the corpus callosum. To confirm that the TTX did not spread to the contralateral hemisphere and that the responsiveness of the contralateral hemisphere was intact, the stimulating electrode was repositioned from the left to the right hemisphere (Fig. 2C, CC-TTX/Stim-R). Stimulation on the right side evoked a strong ipsilateral but a weak contralateral optical response. The absence of a change in the flavoprotein response in both hemispheres shows that the effect of the TTX was restricted to the corpus callosum at the midline and that the contralateral response was mediated by the corpus callosum.

4.3. Changes in blood flow do not account for the flavoprotein responses

We next tested whether changes in blood flow contribute to the flavoprotein autofluorescence responses. The two major pathways mediating increased blood flow in response to neural activity are the neuronal nitric oxide synthase (nNOS) pathway that produces nitric oxide (NO) in response to neural activation and the cyclooxygenase (COX) pathway that produces multiple signaling molecules including prostaglandins in response to astrocyte activation (Hoffmeyer et al. 2007;Kitaura et al. 2007;Attwell et al. 2010). Blocking nitric oxide synthase with L-NAME (1 mM) had no effect on the evoked optical responses in either hemisphere (ipsilateral: $1.50 \pm 0.52\%$ and $1.60 \pm 0.53\%$, baseline and L-NAME, respectively, $F(1,3)=4.34$, $n=4$, $p=0.13$; contralateral: $1.11 \pm 0.37\%$ and $1.16 \pm 0.23\%$, $F(1,3)=0.25$, $p=0.65$). Similarly, blocking cyclooxygenase with indomethacin (100 μM) had no effect (ipsilateral: $2.14 \pm 0.86\%$ and $2.06 \pm 0.82\%$, baseline and indomethacin, respectively, $F(1,3)=0.14$, $n=4$, $p=0.73$; contralateral: $1.48 \pm 0.50\%$ and $1.32 \pm 0.36\%$, $F(1,3)=2.99$, $p=0.18$). These concentrations have been shown to block vasodilatory responses to electrical stimulation in both the cerebral and cerebellar cortex (Ellis et al. 1990;Yang and Iadecola 1998;Shibuki et al. 2003;Toth et al. 2011). Taken together, these data suggest the ipsilateral and contralateral flavoprotein responses are not due to vasodilation, but are neuronal in origin.

4.4. Mapping of local field potentials and flavoprotein signals

To determine the relationship between the evoked optical and neuronal responses, electrophysiological mapping experiments were performed. After recording the optical responses, extracellular field potentials were obtained at several lateral-medial locations across the contralateral optical response. As shown for an example mapping study (Fig. 3A–C), the larger amplitude field potentials (#4–6) were recorded near the center of the optical response and the smaller amplitude field potentials further from the response center. To quantify this relationship, the response amplitude (F/F_0) at the site of the field potential recording was regressed against the peak of the initial negativity (see Materials and Methods). This initial negativity reflects the excitatory synaptic potential (Hoffmeyer et al. 2007). The coefficient of variation (R^2) for the example experiment was 0.96 (blue symbols and regression line in Fig. 3D, F-statistic, $p < 0.001$), confirming a robust linear relation between the optical and field potential recordings. A significant linear relation was observed in all four animals (Fig. 3D). Therefore, the change in flavoprotein fluorescence is strongly coupled to the underlying neuronal activity, specifically the evoked excitatory post-synaptic response.

4.5. Flavoprotein autofluorescence detects both excitation and inhibition

Both local intracortical and transcallosal projections can also activate inhibitory interneurons in the cortex. Much of this inhibition is GABAergic and generates a center-surround pattern of excitation-inhibition, respectively (Derdikman et al. 2003;Helmstaedter et al. 2009;Fino and Yuste 2011). Typically, defining this center-surround organization has relied on electrophysiological mapping. Because flavoprotein imaging monitors both increases and decreases in neuronal activity in the cerebellar cortex (Gao et al. 2006;Reinert et al. 2007;Reinert et al. 2011), we tested whether the flavoprotein response could detect the

inhibitory surround organization in the cerebral cortex. However, train stimulation or single pulse stimulation with a 1 s interval evoked only an increase in fluorescence. We reasoned that the large and long lasting increase in fluorescence at these stimulation parameters might obscure a smaller decrease in fluorescence that reflects synaptic inhibition. Therefore, to better distinguish between excitation and inhibition, stimulation with a single pulse at a 20 s interval was used.

In both the ipsilateral and contralateral hemispheres, the single pulse stimulation protocol evoked a central region of increased fluorescence surrounded by a fluorescence decrease (Fig. 4). The surrounding decrease in fluorescence had a latency of about 0.4–0.6 s, peaked about 1 s, and evolved into a fluorescence increase (Fig. 4A, B and C). Because of the bimodal temporal profile of the optical responses, we quantified both an early and late phase to capture the fluorescence decrease of the surround and the fluorescence increase of the center (Fig. 4B and C). In FVB control mice, the early phase ipsilateral and contralateral responses in the surround region exhibited a decrease in F/F_0 relative to baseline and differed from the fluorescence change in the center (ipsilateral: $F(3,9)=62.18$, n=4, p < 0.0001; contralateral: $F(3,9)=21.99$, p=0.0002, Bonferroni, p < 0.01 for both sides). During the late phase, the surround regions evolved into a fluorescence increase in both hemispheres (Fig. 4E).

We hypothesized and tested whether the surround decrease in fluorescence was due to synaptic inhibition and mediated by $GABA_A$ receptors. Addition of the $GABA_A$ antagonist, Gabazine (1 μM), to the optical recording chamber completely blocked the surround decrease in fluorescence (Fig. 4A). In addition, Gabazine expanded the area of increased fluorescence and decreased the latency (Fig. 4A, B, and C). The population data (Fig. 4D and E) show that the early phase surround decreases in fluorescence were abolished and converted into fluorescence increases in both hemispheres (ipsilateral: $F(3,9)=62.18$, n=4, p < 0.0001; contralateral: $F(3,9)=21.99$, p=0.0002, Bonferroni, p < 0.01). Similarly, during the early phase the center fluorescence increased in both hemispheres (Bonferroni, p < 0.01).

During the late phase (Fig. 4E), Gabazine increased the surround response in both hemispheres and the amplitude of the central response in the contralateral hemisphere (ipsilateral $F(3,9)=9.13$, p=0.0043 and contralateral $F(3,9)=10.12$, p=0.0031, Bonferroni, p < 0.01). However, the amplitude of the ipsilateral center response during the later phase did not change (Bonferroni, p=0.083). These findings are consistent with single pulse stimulation generating GABA synaptic inhibition both around the site of stimulation and the surrounding area.

4.6. Flavoprotein imaging in Mbnl2 KO mice

We used the intracortical stimulation assay to assess the cerebral cortical circuitry in the *Mbnl2* KO mouse model of DM developed by Swanson and colleagues (Charizanis et al. 2012). These experiments used 8 *Mbnl2* KO and 7 littermate C57Bl/6 wild-type mice. The peak amplitude of the response to 10 Hz intracortical stimulation in *Mbnl2* KO mice did not differ from controls (Fig. 5A and B), both ipsilaterally ($F(1,13)=0.44$, p=0.5174) and contralaterally ($F(1,13)=0.11$, p=0.7463). However, two aspects of the response to 10 Hz stimulation differed from wild-type mice. First, the response duration was increased in

Mbnl2 KO mice. As shown in the example images and time course plots (Fig. 5A and C), the duration of the increased fluorescence was prolonged compared to littermate C57Bl/6 wild-type controls. Response duration was quantified as the half-width of the increased fluorescence. Ipsilaterally, the response duration was 4.78 ± 3.93 s *Mbnl2* KO versus 1.86 ± 0.48 s wild-type mice, and contralaterally 4.58 ± 3.96 s and 1.96 ± 0.52 s, respectively and differed significantly in *Mbnl2* KO versus control mice in both hemispheres (ipsilateral: $F(1,13)=4.99$, $p=0.043$; contralateral: $F(1,13)=6.66$, $p=0.023$). This finding suggests an increase in excitability in the cerebral cortex to intracortical stimulation.

In *Mbnl2* KO mice, 10 Hz stimulation also evoked a larger area of activation. As shown in example experiments (Fig. 6A) in *Mbnl2* KO mice intracortical stimulation resulted in larger regions of activation than in wild-type animals in which the fluorescence increase was typically confined to a region surrounding the stimulation site and the mirror region in the contralateral hemisphere. In *Mbnl2* KO mice, the activation typically included a posterior region bilaterally along the midline that was most evident at longer latencies (Fig. 6A). These regions in the parietal lobes correspond approximately to the retrosplenial cortex (Vogt and Peters 1981; Paxinos 2003). To quantify these additional sites of activation, rectangular ROIs (Ip-Ex and Co-Ex, 0.8×1.4 mm) were placed bilaterally centered 0.7mm lateral and 2.2mm posterior from bregma, and the average F/F_0 from 5–7 s after stimulation onset calculated (Fig. 6A). *Mbnl2* KO mice exhibited increased fluorescence in these regions bilaterally compared to wild-type animals (ipsilateral: $F(1,13)=5.37$, $p=0.037$; contralateral: $F(1,13)=6.18$, $p=0.027$, Fig. 6B). As observed for response duration in *Mbnl2* KO mice, there was increased variability as shown in the frequency distribution of the fluorescence changes in the extra regions (Fig. 6C and D). Therefore, 10 Hz intracortical simulation in *Mbnl2* KO mice increases response duration and activates additional cortical areas. While statistically significant, these two aspects of the responses to 10 Hz stimulation also demonstrate increased variability.

We also evaluated the responses to single pulse stimulation in *Mbnl2* KO and C57Bl/6 wild-type mice. As shown for a representative *Mbnl2* KO mouse, both an increased center response and a reduced inhibitory-like surround to single pulse stimulation was observed (Fig. 7A and B). In the overall population data (WT=7, KO=8), the contralateral surround was significantly reduced during the early phase in *Mbnl2* KO mice (Fig. 7C, $F(2,13)=39.06$, $p < 0.001$, Bonferroni $p < 0.01$), and the center of the ipsilateral response during the late phase was significantly increased (Fig. 7C, $F(2,13)=35.39$, $p < 0.001$, Bonferroni $p < 0.01$). Taken together, these results suggest that both train and single pulse stimulations produce stronger excitation and less inhibition in *Mbnl2* KO mice.

4.7. Flavoprotein imaging in Mbnl1-OE mice

A major theory of pathogenesis in DM is that the abnormal RNA transcripts sequester splicing factors, particularly MBNL proteins (Cardani et al. 2006;Lee and Cooper 2009;Du et al. 2010;Charizanis et al. 2012). Conversely, restoring splicing factors has been proposed as a therapeutic approach to mitigate the process. Mice engineered to overexpress human MBNL1 (MBNL1-OE) were shown to reverse the skeletal muscle abnormalities (Chamberlain and Ranum 2012). However, whether MBNL1 overexpression had effects on

the central nervous system was not evaluated. Therefore, we next examined the optical responses to intracortical stimulation to determine if overexpression of MBNL1 affects cerebral cortical circuitry.

We tested two MBNL1-OE lines: L14686 (n=8 FVB wild-type and OE, each); and L15132 (n=6 FVB wild-type, and n=7 OE). Overexpression of MBNL1 was verified by western blot analysis in both MBNL1-OE lines (Fig. 8A). Stimulation with a 10 Hz train revealed a reduction in the contralateral response in both lines as illustrated in Fig. 8B and C from a representative FVB wild-type and MBNL1-OE mouse (L14686). Stimulation in the motor cortex of L14686 on either the right or left motor cortex evoked a significant smaller response ($0.62 \pm 0.36\%$ F/F_0) in the contralateral hemisphere compared to a wild-type control ($1.03 \pm 0.38\%$ F/F_0; $F(1,14)=7.39$, $p=0.017$). Despite the reduction in the contralateral hemisphere, the ipsilateral response was unchanged in L14686 (Fig. 8D). The selective reduction for the contralateral response compared to wild-type mice was also observed in L15132 (1.37 ± 0.26 vs $1.01 \pm 0.31\%$ F/F_0, $F(1, 11)=10.25$, $p < 0.01$), as the ipsilateral response amplitude did not differ for either MBNL1-OE line (for L14686: $F(1,14)=0.08$, $p=0.7853$; and for L15132: $F(1,11)=0.96$, $p=0.3486$). This result suggests a possible deficit in corpus callosum transmission.

Finally, we tested the response to single pulse stimulation in both MBNL1-OE lines: L14686 (n=6 FVB wild-type, and n=5 OE); and L15132 (n=7 FVB wild-type and OE, each). The inhibitory-like surround observed above in FVB mice was markedly reduced in MBNL1-OE mice, as shown in the example experiment (Figs. 9A and B). The surround decrease in fluorescence was much less evident in both hemispheres from the L14686 line compared to control. Consistent with the decrease in surround inhibition, there was a significant increase in fluorescence in the center of the response in both hemispheres of the MBNL1-OE mouse. The population results show that the inhibitory-like surround during the early phase was significantly different from the controls in L14686 (ipsilateral: $F(2, 9)=27.92$, $p < 0.0001$, contralateral: $F(2, 9)=138.65$, $p < 0.0001$, Bonferonni, $p < 0.01$), and the contralateral surround in L15132 (contralateral: $F(2, 12)=74.69$, $p < 0.0001$, Bonferonni, $p < 0.05$). Additionally, the response in all ROIs were greater in the late phase in both hemispheres for both L14686 (ipsilateral: $F(2,9)=97.28$, $p < 0.0001$, contralateral: $F(2,9)=24.53$, $p=0.0002$, Bonferonni, $p < 0.01$ for both sides) and in L1532 (ipsilateral: $F(2,12)=147.7$, $p < 0.0001$, contralateral $F(2,12)=53.8$, $p < 0.0001$, Bonferonni, $p < 0.01$ for both sides). Therefore, the normal GABAergic inhibition evoked by intracortical and corpus callosum stimulation was reduced in MBNL1-OE mice.

5. Discussion

5.1. Major findings

In this study, we demonstrated that flavoprotein imaging can be used to map neuronal activity in response to intracortical stimulation of the mouse cerebral cortex. The mesoscopic capabilities of flavoprotein imaging (Cramer et al. 2015;Ma et al. 2016;Kozberg et al. 2016) allowed us to image large regions of the exposed cerebral cortex including the intra- and intercortical responses to intracortical stimulation. Train stimulation of the motor cortex resulted in both an ipsilateral and contralateral increase in flavoprotein fluorescence and the

latter was mediated by neuronal activation through the corpus callosum. Stimulation with only a single pulse revealed a center-surround type pattern of excitation-inhibition. *Mbnl2* KO mice exhibited an increased excitability to intracortical train stimulation, with longer duration responses, activation of additional regions, and a lack of center-surround pattern of inhibition to single pulse stimulation. Overexpression of MBNL1 revealed a weaker contralateral response, and a lack of inhibitory-like surround response. Thus, flavoprotein imaging reveals several changes in cerebral cortical circuits in these two DM-related mouse models.

5.2. Neuronal basis for flavoprotein response

Stimulation of the motor cortex at 10 Hz resulted in ipsilateral and contralateral responses that consisted of a central region of increased fluorescence, consistent with previous reports in the mouse cerebral cortex (Hishida et al. 2011). TTX abolished the responses, demonstrating that the response was primarily neuronal and that action potentials were extensively involved in activating both the neighboring ipsilateral cortex and contralateral hemisphere. A large fraction of the fluorescence increase was due to postsynaptic activation of neurons as blocking ionotropic glutamate receptors greatly reduced both the ipsilateral and contralateral responses. However, it is likely that mechanisms other than ionotropic glutamatergic synaptic transmission contribute to the fluorescence increase, as only ~53 ± 9% was blocked ipsilaterally and ~74 ± 7% blocked contralaterally by APV and DNQX. While the ipsilateral response is likely to involve direct activation of neurons that would not be blocked by ionotropic glutamatergic antagonists, direct electrical activation cannot account for the remaining 25% not blocked in the contralateral hemisphere. Several other classes of excitatory synaptic transmission or post-synaptic receptors may contribute, including metabotropic glutamate receptor types 1 and 5, as both are involved in the cerebral cortical circuitry (Ferraguti and Shigemoto 2006;Alexander and Godwin 2006).

Another potential contributor to the flavoprotein signal is changes in blood flow and/or blood oxygenation. The two major mediators of increasing cerebral blood flow, the nNOS and cyclooxygenase (COX) pathways respectively, account for ~85% of the increase in blood flow that accompanies neuronal activation (Hoffmeyer et al. 2007;Kitaura et al. 2007;Attwell et al. 2010). Blocking either of these two pathways had no significant effect on the optical responses, showing that the vast majority of the changes in flavoprotein fluorescence was not mediated by changes in blood flow. The lack of a significant blood flow contribution to the flavoprotein signal is consistent with previous findings in several species in both the cerebellum and cerebral cortex of anesthetized animals (Shibuki et al. 2003;Reinert et al. 2004;Husson et al. 2007;Reinert et al. 2007).

Single pulse stimulation evoked a more complex pattern characterized by a central region of increased fluorescence surrounded by decreased fluorescence. The latter region is consistent with surround inhibition, as blocking GABA$_A$ receptors converted the fluorescence decrease into an increase. While surround inhibition is considered a fundamental feature of the neocortical architecture and shapes information processing (Krimer and Goldman-Rakic 2001;Kremkow et al. 2010;Isaacson and Scanziani 2011), most studies of surround inhibition used electrophysiological recordings that have some limitations in revealing the

spatial characteristics. An advantage of flavoprotein imaging is the ability to provide a relatively high resolution spatial map. Previous work showed that patches of decreased fluorescence in the cerebellar cortex evoked by parallel fiber stimulation are due to $GABA_A$ inhibition (Gao et al. 2006). To our knowledge, this is the first report using flavoprotein imaging to monitor both excitation and inhibition in the cerebral cortex, further extending the utility of this technique.

5.3. Involvement of the corpus callosum

The corpus callosum is the largest commissural tract in the human brain and connects the cerebral hemispheres (Paul et al. 2007;Edwards et al. 2014;Fenlon and Richards 2015). Originating primarily from neurons in the cortical layers II/III and layer V of the neocortex, callosal axons project to equivalent locations in the contralateral cortex (Wahl et al. 2007;Wahl et al. 2009). An essential pathway for transfer of interhemispheric information, callosal axons are excitatory and synapse both on excitatory neurons in the contralateral cortex and also on inhibitory interneurons. These precise homotopic patterns of connections play important roles in coordination of cortical functions, including motor, sensory and cognitive processes (Paul et al. 2007;Edwards et al. 2014). In our results, the properties of the activated region in the contralateral hemisphere were similar to the ipsilateral response following either 10 Hz train or single pulse stimulation in naïve wild-type mice. While these properties are consistent with the contralateral increase in fluorescence being mediated by the corpus callosum, a more definitive test was that small volumes (~30–35 nL) of TTX injected into the corpus callosum at the midline abolished the contralateral response, yet the ipsilateral response remained unchanged.

There has been a long standing debate as whether the primary function of the corpus callosum is to excite or inhibit the opposite hemisphere (Cook 1984;Yazgan et al. 1995;Bloom and Hynd 2005). While the present study was not designed to answer this question, the results do show that the level of excitation or inhibition is likely dependent on the pattern of corpus callosum activation. Furthermore, altering the expression of MBNL splicing factor changes the balance of excitation and inhibition evoked by corpus callosum transmission.

5.4. Flavoprotein imaging in the Mbnl2 KO model of myotonic dystrophy

Both the ipsilateral and contralateral responses to intracortical stimulation were used to investigate mouse models relevant to DM pathogenesis. The *Mbnl2* KO mouse model recapitulates many key disease features (Charizanis et al. 2012). Several differences in the responses to intracortical stimulation were observed in this model. Longer duration responses and activation of additional cortical regions characterized 10 Hz stimulation in *Mbnl2* KO mice. The normal surround inhibition evoked by stimulation with a single pulse was absent in *Mbnl2* KO mice and there was a concomitant increase in the excitatory component of the response. These changes were present bilaterally and together imply increased cortical responsiveness to direct stimulation. This increased responsiveness is consistent with the augmented seizure susceptibility observed in *Mbnl2* KO mice (Charizanis et al. 2012) and in the DMSXL transgenic model of DM that expresses a human *DMPK* transgene with CTG expansion ranging from 1200–1700 in length (Gomes-Pereira et

al. 2007). There have been a small number of case reports showing comorbidity of epilepsy in DM1 (Worku 2014;Kajal et al. 2017) and DM2 (Cagnetti et al. 2014;Giuliano et al. 2016), however there has been no definitive link between increased seizure susceptibility and DM. It has also been reported that increased neurosecretion occurs in cell cultures expressing toxic CUG repeats (Hernandez-Hernandez et al. 2013). Together these observations support the hypothesis that DM has characteristics of an altered excitability disorder (Charizanis et al. 2012), however, not necessarily producing a seizure disorder (Yayla et al. 2017).

The engagement of additional cortical areas with intracortical stimulation, specifically the retrosplenial cortex, is intriguing in that the retrosplenial cortex is involved in several cognitive functions including navigation, episodic memory, imagination, and planning for the future (Vann et al. 2009). Abnormal circuitry function and information processing in the retrosplenial cortex could contribute to abnormalities in these behaviors observed in DM patients. However, we add that to our knowledge, there are no reports of retrosplenial involvement in DM1 or DM2. Given this important caveat, the abnormal responses in *Mbnl2* KO mice highlight that the changes in splicing factors associated with DM alter cerebral cortical functional connectivity.

The present *in vivo* results when taken together with previous findings suggest complex changes in synaptic functioning in the *Mbnl2* KO mice. *Mbnl2* KO mice also exhibit decreased NMDA-mediated receptor potentials and long-term potentiation in CA1 pyramid cells of the hippocampus (Charizanis et al. 2012). This complexity is expected given the widespread effect of knocking out *Mbnl2* on alternative splicing, including key genes encoding ion channels and synaptic function. For example, adult exon skipping occurs for *Cacna1d* ($Ca_v1.3$) that codes for the voltage-gated L-type calcium channel, and *Kcnma1* that codes for a large conductance calcium-activated potassium channel (Charizanis et al. 2012). Additionally, increased inclusion of exon 5 of *Grin1*, coding for the NMDA receptor type 1 subunit, occurs in *Mbnl2* KO mice (Charizanis et al. 2012), which has been reported to decrease dendritic localization (Pal et al. 2003). Persistence of the fetal or misspliced forms of any or a combination of these channels is likely to alter excitability of cortical circuits, as we observed. Furthermore, the developmental splicing defects can be regional as is the fetal pattern. For example, the splicing pattern for *Kcnma1* exon 25a differed substantially in the forebrain versus the hindbrain in *Mbnl2* KO mice (Charizanis et al. 2012). Therefore, DM is likely to have differential effects on excitability and synaptic function depending on CNS location.

Of note, there is an alteration in skeletal muscle glucose metabolism in DM1 and DM2 due to increased levels of pyruvate kinase M2 (PKM2) (Gao and Cooper 2013). While *Mbnl1; Mbnl2* double KO mice show a significant shift towards exon 10 inclusion and increased PKM2 expression, the *Mbnl2* KO brain does not (Charizanis et al. 2012). Therefore, the changes in flavoprotein responses reported here are unlikely to be the result of aberrant PKM2 upregulation and altered glucose metabolism.

5.5. Effects of MBNL1 overexpression

The sequestration of MBNL1 by CUG and CCUG transcripts is likely to play a major role in the splicing abnormalities and the multi-systemic abnormalities in DM (Novak et

al. 2000;Kanadia et al. 2003;Yuan et al. 2007;Du et al. 2010). Therefore, upregulation of MBNL1 is a potential therapeutic strategy for DM. A previous study of transgenic mouse lines (including L14686 mice) demonstrated that overexpression of MBNL1 is well-tolerated in skeletal muscle and MBNL1 overexpression prevents CUG-induced myotonia (Chamberlain and Ranum 2012). A recent report also demonstrated that restoring endogenous levels of MBNL proteins decreased missplicing events and restored pathological symptoms in a *Drosophila* DM1 model (Cerro-Herreros et al. 2016). While a promising strategy, the effect of overexpression in the CNS requires investigation. The present results showed that MBNL1 overexpression altered cerebral cortical responsiveness by decreasing the response in the contralateral hemisphere evoked by 10 Hz train stimulation. Given that there was no change in the ipsilateral response, the decreased contralateral response may reflect altered corpus callosum function. As reviewed earlier (see Introduction), white matter and functional connectivity changes in DM1 and DM2 patients, including in the corpus callosum, have been a common finding in anatomical and DTI studies (Fukuda et al. 2005;Ota et al. 2006;Wozniak et al. 2011;Minnerop et al. 2011;Franc et al. 2012;Serra et al. 2014;Serra et al. 2016). However, we would emphasize that the decreased flavoprotein response in the contralateral hemisphere is not definitive for abnormal corpus callosum function, with additional experiments needed to test other possibilities. For example, MBNL1-OE mice also showed a reduction in the inhibitory-like surround in both hemispheres, consistent with a more general change in synaptic function.

MBNL1-OE mice showed decreased responses to corpus callosum stimulation that in theory could counteract the increased responsiveness observed in *Mbnl2* KO animals. However, overexpression of MBNL1 did not result in a simple reversal of the changes observed in *Mbnl2* KO mice. The wild-type center-surround pattern of inhibition was reduced in both mouse models. Interestingly, there is a modest increase in the expression of MBNL1 in *Mbnl2* KO mice (Charizanis et al. 2012) that could account for the decreased inhibitory-like surround observed in the two mouse models. These findings reinforce the complexity introduced with changes in the expression of these important splicing factors.

Acknowledgments

References

Alexander GM, Godwin DW. 2006; Metabotropic glutamate receptors as a strategic target for the treatment of epilepsy. Epilepsy Res. 71 :1–22. [PubMed: 16787741]

Antonini G, Mainero C, Romano A, Giubilei F, Ceschin V, Gragnani F, Morino S, Fiorelli M, Soscia F, Di PA, Caramia F. 2004; Cerebral atrophy in myotonic dystrophy: a voxel based morphometric study. J Neurol Neurosurg Psychiatry. 75 :1611–1613. [PubMed: 15489397]

Attwell D, Buchan AM, Charpak S, Lauritzen M, MacVicar BA, Newman EA. 2010; Glial and neuronal control of brain blood flow. Nature. 468 :232–243. [PubMed: 21068832]

Bloom JS, Hynd GW. 2005; The role of the corpus callosum in interhemispheric transfer of information: excitation or inhibition? Neuropsychol Rev. 15 :59–71. [PubMed: 16211466]

Brennan AM, Connor JA, Shuttleworth CW. 2006; NAD(P)H fluorescence transients after synaptic activity in brain slices: predominant role of mitochondrial function. J Cereb Blood Flow Metab. 26 :1389–1406. [PubMed: 16538234]

Brook JD, McCurrach ME, Harley HG, Buckler AJ, Church D, Aburatani H, Hunter K, Stanton VP, Thirion JP, Hudson T. 1992; Molecular basis of myotonic dystrophy: expansion of a trinucleotide (CTG) repeat at the 3′ end of a transcript encoding a protein kinase family member. Cell. 69 :385.

Cagnetti C, Buratti L, Foschi N, Balestrini S, Provinciali L. 2014; Generalized epilepsy in a patient with myotonic dystrophy type 2. Neurol Sci. 35 :489–490. [PubMed: 24277201]

Cardani R, Mancinelli E, Rotondo G, Sansone V, Meola G. 2006; Muscleblind-like protein 1 nuclear sequestration is a molecular pathology marker of DM1 and DM2. Eur J Histochem. 50 :177–182. [PubMed: 16920640]

Cerro-Herreros E, Fernandez-Costa JM, Sabater-Arcis M, Llamusi B, Artero R. 2016; Derepressing muscleblind expression by miRNA sponges ameliorates myotonic dystrophy-like phenotypes in Drosophila. Sci Rep. 6 :36230. [PubMed: 27805016]

Chamberlain CM, Ranum LP. 2012; Mouse model of muscleblind-like 1 over-expression: skeletal muscle effects and therapeutic promise. Hum Mol Genet. 21 :4645–4654. [PubMed: 22846424]

Chance B. 1991; Optical method. Annu Rev Biophys Biophys Chem. 20 :1–28. [PubMed: 1867711]

Charizanis K, et al. 2012; Muscleblind-like 2-mediated alternative splicing in the developing brain and dysregulation in myotonic dystrophy. Neuron. 75 :437–450. [PubMed: 22884328]

Chovsepian A, Empl L, Correa D, Bareyre FM. 2017; Heterotopic transcallosal projections are present throughout the mouse cortex. Front Cell Neurosci. 11 :36. [PubMed: 28270750]

Cook ND. 1984; Homotopic Callosal Inhibition. Brain. 23 :116–125.

Coutinho V, Mutoh H, Knopfel T. 2004; Functional topology of the mossy fibre-granule cell—Purkinje cell system revealed by imaging of intrinsic fluorescence in mouse cerebellum. Eur J Neurosci. 20 :740–748. [PubMed: 15255984]

Cramer SW, Gao W, Chen G, Ebner TJ. 2013; Reevaluation of the beam and radial hypotheses of parallel fiber action in the cerebellar cortex. J Neurosci. 33 :11412–11424. [PubMed: 23843513]

Cramer SW, Popa LS, Carter RE, Chen G, Ebner TJ. 2015; Abnormal excitability and episodic low frequency oscillation in the cerebral cortex of the *tottering* mouse. J Neurosci. 35 :5664–5679. [PubMed: 25855180]

Derdikman D, Hildesheim R, Ahissar E, Arieli A, Grinvald A. 2003; Imaging spatiotemporal dynamics of surround inhibition in the barrels somatosensory cortex. J Neurosci. 23 :3100–3105. [PubMed: 12716915]

Du H, Cline MS, Osborne RJ, Tuttle DL, Clark TA, Donohue JP, Hall MP, Shiue L, Swanson MS, Thornton CA, Ares M Jr. 2010; Aberrant alternative splicing and extracellular matrix gene expression in mouse models of myotonic dystrophy. Nat Struct Mol Biol. 17 :187–193. [PubMed: 20098426]

Edwards TJ, Sherr EH, Barkovich AJ, Richards LJ. 2014; Clinical, genetic and imaging findings identify new causes for corpus callosum development syndromes. Brain. 137 :1579–1613. [PubMed: 24477430]

Ellis EF, Police RJ, Yancey L, McKinney JS, Amruthesh SC. 1990; Dilation of cerebral arterioles by cytochrome P-450 metabolites of arachidonic acid. Am J Phys. 259 :H1171–H1177.

Fenlon LR, Richards LJ. 2015; Contralateral targeting of the corpus callosum in normal and pathological brain function. Trends Neurosci. 38 :264–272. [PubMed: 25841797]

Ferraguti F, Shigemoto R. 2006; Metabotropic glutamate receptors. Cell Tissue Res. 326 :483–504. [PubMed: 16847639]

Fino E, Yuste R. 2011; Dense inhibitory connectivity in neocortex. Neuron. 69 :1188–1203. [PubMed: 21435562]

Franc DT, Muetzel RL, Robinson PR, Rodriguez CP, Dalton JC, Naughton CE, Mueller BA, Wozniak JR, Lim KO, Day JW. 2012 Cerebral and Muscle MRI Abnormalities in Myotonic Dystrophy. Neuromuscul Disord.

Fu YH, Pizzuti A, Fenwick RG Jr, King J, Rajnarayan S, Dunne PW, Dubel J, Nasser GA, Ashizawa T, de Jong P. 1992; An unstable triplet repeat in a gene related to myotonic muscular dystrophy. Science. 255 :1256–1258. [PubMed: 1546326]

Fukuda H, Horiguchi J, Ono C, Ohshita T, Takaba J, Ito K. 2005; Diffusion tensor imaging of cerebral white matter in patients with myotonic dystrophy. Acta Radiol. 46 :104–109. [PubMed: 15841748]

Gao Z, Cooper TA. 2013; Reexpression of pyruvate kinase M2 in type 1 myofibers correlates with altered glucose metabolism in myotonic dystrophy. Proc Natl Acad Sci U S A. 110 :13570–13575. [PubMed: 23901116]

Gao W, Chen G, Reinert KC, Ebner TJ. 2006; Cerebellar cortical molecular layer inhibition is organized in parasagittal zones. J Neurosci. 26 :8377–8387. [PubMed: 16899733]

Gaul C, Schmidt T, Windisch G, Wieser T, Muller T, Vielhaber S, Zierz S, Leplow B. 2006; Subtle cognitive dysfunction in adult onset myotonic dystrophy type 1 (DM1) and type 2 (DM2). Neurology. 67 :350–352. [PubMed: 16864839]

Giuliano L, Sofia V, Cardani R, Meola G, Zappia M. 2016; Drug resistant focal epilepsy in a patient with myotonic dystrophy type 2: casual or causal association? Neurol Sci. 37 :1867–1868. [PubMed: 27225277]

Gomes-Pereira M, Foiry L, Nicole A, Huguet A, Junien C, Munnich A, Gourdon G. 2007; CTG trinucleotide repeat "big jumps": large expansions, small mice. PLoS Genet. 3 :e52. [PubMed: 17411343]

Haley MS, Fontanini A, Maffei A. 2016; Laminar- and target-specific amygdalar inputs in rat primary gustatory cortex. J Neurosci. 36 :2623–2637. [PubMed: 26937004]

Harper, PS. Myotonic Dystrophy. 3. W. B. Saunders; London: 2001.

Helmstaedter M, Sakmann B, Feldmeyer D. 2009; Neuronal correlates of local, lateral, and translaminar inhibition with reference to cortical columns. Cereb Cortex. 19 :926–937. [PubMed: 18832335]

Hernandez-Hernandez O, et al. 2013; Myotonic dystrophy CTG expansion affects synaptic vesicle proteins, neurotransmission and mouse behaviour. Brain. 136 :957–970. [PubMed: 23404338]

Hishida R, Watanabe K, Kudoh M, Shibuki K. 2011; Transcranial electrical stimulation of cortico-cortical connections in anesthetized mice. J Neurosci Methods. 201 :315–321. [PubMed: 21864574]

Hoffmeyer HW, Enager P, Thomsen KJ, Lauritzen MJ. 2007; Nonlinear neurovascular coupling in rat sensory cortex by activation of transcallosal fibers. J Cereb Blood Flow Metab. 27 :575–587. [PubMed: 16896350]

Husson TR, Mallik AK, Zhang JX, Issa NP. 2007; Functional imaging of primary visual cortex using flavoprotein autofluorescence. J Neurosci. 27 :8665–8675. [PubMed: 17687044]

Isaacson JS, Scanziani M. 2011; How inhibition shapes cortical activity. Neuron. 72 :231–243. [PubMed: 22017986]

Kajal, HL, Singh, CP, Garg, R. Myotonic Dystrophy and Epilepsy. 2017. 343–344.

Kanadia RN, Johnstone KA, Mankodi A, Lungu C, Thornton CA, Esson D, Timmers AM, Hauswirth WW, Swanson MS. 2003; A muscleblind knockout model for myotonic dystrophy. Science. 302 :1978–1980. [PubMed: 14671308]

Kassubek J, Juengling FD, Hoffmann S, Rosenbohm A, Kurt A, Jurkat-Rott K, Steinbach P, Wolf M, Ludolph AC, Lehmann-Horn F, Lerche H, Weber YG. 2003; Quantification of brain atrophy in patients with myotonic dystrophy and proximal myotonic myopathy: a controlled 3-dimensional magnetic resonance imaging study. Neurosci Lett. 348 :73–76. [PubMed: 12902021]

Keller A. 1993; Intrinsic synaptic organization of the motor cortex. Cereb Cortex. 3 :430–441. [PubMed: 8260811]

Kitaura H, Uozumi N, Tohmi M, Yamazaki M, Sakimura K, Kudoh M, Shimizu T, Shibuki K. 2007; Roles of nitric oxide as a vasodilator in neurovascular coupling of mouse somatosensory cortex. Neurosci Res. 59 :160–171. [PubMed: 17655958]

Kozberg MG, Ma Y, Shaik MA, Kim SH, Hillman EM. 2016; Rapid postnatal expansion of neural networks occurs in an environment of altered neurovascular and neurometabolic coupling. J Neurosci. 36 :6704–6717. [PubMed: 27335402]

Kremkow J, Perrinet LU, Masson GS, Aertsen A. 2010; Functional consequences of correlated excitatory and inhibitory conductances in cortical networks. J Comput Neurosci. 28 :579–594. [PubMed: 20490645]

Krimer LS, Goldman-Rakic PS. 2001; Prefrontal microcircuits: membrane properties and excitatory input of local, medium, and wide arbor interneurons. J Neurosci. 21 :3788–3796. [PubMed: 11356867]

Kumar SS, Huguenard JR. 2001; Properties of excitatory synaptic connections mediated by the corpus callosum in the developing rat neocortex. J Neurophysiol. 86 :2973–2985. [PubMed: 11731554]

Lee JE, Cooper TA. 2009; Pathogenic mechanisms of myotonic dystrophy. Biochem Soc Trans. 37 :1281–1286. [PubMed: 19909263]

Lieke EE, Frostig RD, Arieli A, Ts'o DY, Hildesheim R, Grinvald A. 1989; Optical imaging of cortical activity: real-time imaging using extrinsic dye-signals and high resolution imaging based on slow intrinsic-signals. Annu Rev Physiol. 51 :543–559. [PubMed: 2653196]

Liquori CL, Ricker K, Moseley ML, Jacobsen JF, Kress W, Naylor SL, Day JW, Ranum LP. 2001; Myotonic dystrophy type 2 caused by a CCTG expansion in intron 1 of ZNF9. Science. 293 :864–867. [PubMed: 11486088]

Ma Y, Shaik MA, Kim SH, Kozberg MG, Thibodeaux DN, Zhao HT, Yu H, Hillman EM. 2016 Wide-field optical mapping of neural activity and brain haemodynamics: considerations and novel approaches. Philos Trans R Soc Lond Ser B Biol Sci. :371.

Mahadevan M, Tsilfidis C, Sabourin L, Shutler G, Amemiya C, Jansen G, Neville C, Narang M, Barcelo J, O'Hoy K. 1992; Myotonic dystrophy mutation: an unstable CTG repeat in the 3′ untranslated region of the gene. Science. 255 :1253–1255. [PubMed: 1546325]

Meola G, Sansone V, Perani D, Colleluori A, Cappa S, Cotelli M, Fazio F, Thornton CA, Moxley RT. 1999; Reduced cerebral blood flow and impaired visual-spatial function in proximal myotonic myopathy. Neurology. 53 :1042–1050. [PubMed: 10496264]

Meola G, Sansone V, Perani D, Scarone S, Cappa S, Dragoni C, Cattaneo E, Cotelli M, Gobbo C, Fazio F, Siciliano G, Mancuso M, Vitelli E, Zhang S, Krahe R, Moxley RT. 2003; Executive dysfunction and avoidant personality trait in myotonic dystrophy type 1 (DM-1) and in proximal myotonic myopathy (PROMM/DM-2). Neuromuscul Disord. 13 :813–821. [PubMed: 14678804]

Minnerop M, Weber B, Schoene-Bake JC, Roeske S, Mirbach S, Anspach C, Schneider-Gold C, Betz RC, Helmstaedter C, Tittgemeyer M, Klockgether T, Kornblum C. 2011; The brain in myotonic dystrophy 1 and 2: evidence for a predominant white matter disease. Brain. 134 :3530–3546. [PubMed: 22131273]

Mitchell BD, Macklis JD. 2005; Large-scale maintenance of dual projections by callosal and frontal cortical projection neurons in adult mice. J Comp Neurol. 482 :17–32. [PubMed: 15612019]

Modoni A, Silvestri G, Pomponi MG, Mangiola F, Tonali PA, Marra C. 2004; Characterization of the pattern of cognitive impairment in myotonic dystrophy type 1. Arch Neurol. 61 :1943–1947. [PubMed: 15596617]

Novak KE, Miller LE, Houk JC. 2000; Kinematic properties of rapid hand movements in a knob turning task. Exp Brain Res. 132 :419–433. [PubMed: 10912823]

Ono S, Kanda F, Takahashi K, Fukuoka Y, Jinnai K, Kurisaki H, Mitake S, Inagaki T, Nagao K. 1996; Neuronal loss in the medullary reticular formation in myotonic dystrophy: a clinicopathological study. Neurology. 46 :228–231. [PubMed: 8559381]

Ota M, Sato N, Ohya Y, Aoki Y, Mizukami K, Mori T, Asada T. 2006; Relationship between diffusion tensor imaging and brain morphology in patients with myotonic dystrophy. Neurosci Lett. 407 :234–239. [PubMed: 16978781]

Pal R, Agbas A, Bao X, Hui D, Leary C, Hunt J, Naniwadekar A, Michaelis ML, Kumar KN, Michaelis EK. 2003; Selective dendrite-targeting of mRNAs of NR1 splice variants without exon 5: identification of a cis-acting sequence and isolation of sequence-binding proteins. Brain Res. 994 :1–18. [PubMed: 14642443]

Paul LK, Brown WS, Adolphs R, Tyszka JM, Richards LJ, Mukherjee P, Sherr EH. 2007; Agenesis of the corpus callosum: genetic, developmental and functional aspects of connectivity. Nat Rev Neurosci. 8 :287–299. [PubMed: 17375041]

Paxinos, GFKBJ. The Mouse Brain in Stereotaxic Coordinates. Academic Press; 2003.

Reinert KC, Dunbar RL, Gao W, Chen G, Ebner TJ. 2004; Flavoprotein autofluorescence imaging of neuronal activation in the cerebellar cortex *in vivo*. J Neurophysiol. 92 :199–211. [PubMed: 14985415]

Reinert KC, Gao W, Chen G, Ebner TJ. 2007; Flavoprotein autofluorescence imaging in the cerebellar cortex *in vivo*. J Neurosci Res. 85 :3221–3232. [PubMed: 17520745]

Reinert KC, Gao W, Chen G, Wang X, Ebner TJ. 2011; Cellular and metabolic origins of flavoprotein autofluorescence in the cerebellar cortex *in vivo*. Cerebellum. 10 :585–589. [PubMed: 21503591]

Rubinsztein JS, Rubinsztein DC, McKenna PJ, Goodburn S, Holland AJ. 1997; Mild myotonic dystrophy is associated with memory impairment in the context of normal general intelligence. J Med Genet. 34 :229–233. [PubMed: 9132495]

Serra L, Silvestri G, Petrucci A, Basile B, Masciullo M, Makovac E, Torso M, Spano B, Mastropasqua C, Harrison NA, Bianchi ML, Giacanelli M, Caltagirone C, Cercignani M, Bozzali M. 2014; Abnormal functional brain connectivity and personality traits in myotonic dystrophy type 1. JAMA Neurol. 71 :603–611. [PubMed: 24664202]

Serra L, Mancini M, Silvestri G, Petrucci A, Masciullo M, Spano B, Torso M, Mastropasqua C, Giacanelli M, Caltagirone C, Cercignani M, Meola G, Bozzali M. 2016; Brain connectomics' modification to clarify motor and nonmotor features of myotonic dystrophy type 1. Neural Plast. 2016 :2696085. [PubMed: 27313901]

Shibuki K, Hishida R, Murakami H, Kudoh M, Kawaguchi T, Watanabe M, Watanabe S, Kouuchi T, Tanaka R. 2003; Dynamic imaging of somatosensory cortical activity in the rat visualized by flavoprotein autofluorescence. J Physiol. 549 :919–927. [PubMed: 12730344]

Shlosberg D, Amitai Y, Azouz R. 2006; Time-dependent, layer-specific modulation of sensory responses mediated by neocortical layer 1. J Neurophysiol. 96 :3170–3182. [PubMed: 17110738]

van Spaendonck KP, Ter Bruggen JP, Weyn Banningh EW, Maassen BA, Van de Biezenbos JB, Gabreels FJ. 1995; Cognitive function in early adult and adult onset myotonic dystrophy. Acta Neurol Scand. 91 :456–461. [PubMed: 7572040]

Suenaga K, Lee KY, Nakamori M, Tatsumi Y, Takahashi MP, Fujimura H, Jinnai K, Yoshikawa H, Du H, Ares M Jr, Swanson MS, Kimura T. 2012; Muscleblind-like 1 knockout mice reveal novel splicing defects in the myotonic dystrophy brain. PLoS One. 7 :e33218. [PubMed: 22427994]

Toth P, Rozsa B, Springo Z, Doczi T, Koller A. 2011; Isolated human and rat cerebral arteries constrict to increases in flow: role of 20-HETE and TP receptors. J Cereb Blood Flow Metab. 31 :2096–2105. [PubMed: 21610722]

Vann SD, Aggleton JP, Maguire EA. 2009; What does the retrosplenial cortex do? Nat Rev Neurosci. 10 :792–802. [PubMed: 19812579]

Vogt BA, Peters A. 1981; Form and distribution of neurons in rat cingulate cortex: areas 32, 24, and 29. J Comp Neurol. 195 :603–625. [PubMed: 7462444]

Wahl M, Lauterbach-Soon B, Hattingen E, Jung P, Singer O, Volz S, Klein JC, Steinmetz H, Ziemann U. 2007; Human motor corpus callosum: topography, somatotopy, and link between microstructure and function. J Neurosci. 27 :12132–12138. [PubMed: 17989279]

Wahl M, Strominger Z, Jeremy RJ, Barkovich AJ, Wakahiro M, Sherr EH, Mukherjee P. 2009; Variability of homotopic and heterotopic callosal connectivity in partial agenesis of the corpus callosum: a 3T diffusion tensor imaging and Q-ball tractography study. AJNR Am J Neuroradiol. 30 :282–289. [PubMed: 19001538]

Wang X, Chen G, Gao W, Ebner TJ. 2011; Parasagittally aligned, mGluR1-dependent patches are evoked at long latencies by parallel fiber stimulation in the mouse cerebellar cortex *in vivo*. J Neurophysiol. 105 :1732–1746. [PubMed: 21289138]

Worku DK. 2014; Concurrence of myotonic dystrophy and epilepsy: a case report. J Med Case Rep. 8 :427. [PubMed: 25496057]

Wozniak JR, Mueller BA, Ward EE, Lim KO, Day JW. 2011; White matter abnormalities and neurocognitive correlates in children and adolescents with myotonic dystrophy type 1: a diffusion tensor imaging study. Neuromuscul Disord. 21 :89–96. [PubMed: 21169018]

Yang G, Iadecola C. 1998; Activation of cerebellar climbing fibers increases cerebellar blood flow: role of glutamate receptors, nitric oxide, and cGMP. Stroke. 29 :499–507. [PubMed: 9472896]

Yayla V, Bajrami A, Azman F, Sozer N, Cagirici S. 2017; P219 Cortical Excitability in Dystrophia Myotonica Type. 1 :e248–e249.

Yazgan MY, Wexler BE, Kinsbourne M, Peterson B, Leckman JF. 1995; Functional significance of individual variations in callosal area. Neuropsychologia. 33 :769–779. [PubMed: 7675166]

Yuan Y, Compton SA, Sobczak K, Stenberg MG, Thornton CA, Griffith JD, Swanson MS. 2007; Muscleblind-like 1 interacts with RNA hairpins in splicing target and pathogenic RNAs. Nucleic Acids Res. 35 :5474–5486. [PubMed: 17702765]
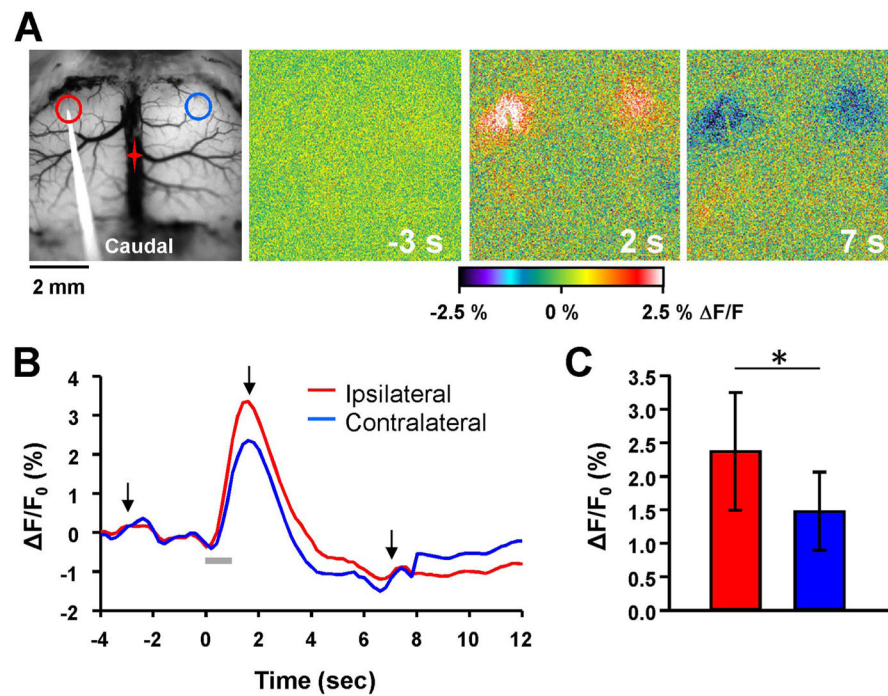
Fig. 1.

Flavoprotein autofluorescence responses to intracortical stimulation. A. Example background and pseudocolored images of the motor cortex in an FVB mouse during a 10 Hz train stimulation for 1 s. Red and blue circles denote regions of interest (ROIs) for calculating peak autofluorescence changes on the ipsilateral and contralateral hemispheres, respectively. In this and all subsequent figures, the red star indicates the location of bregma. B. Time course of the flavoprotein autofluorescence change in response to the 10 Hz stimulation (gray bar). Arrows denote times at which images from *A* were taken. C. Quantification of the peak flavoprotein autofluorescence response on the ipsilateral (red) and contralateral (blue) hemisphere (n=15).
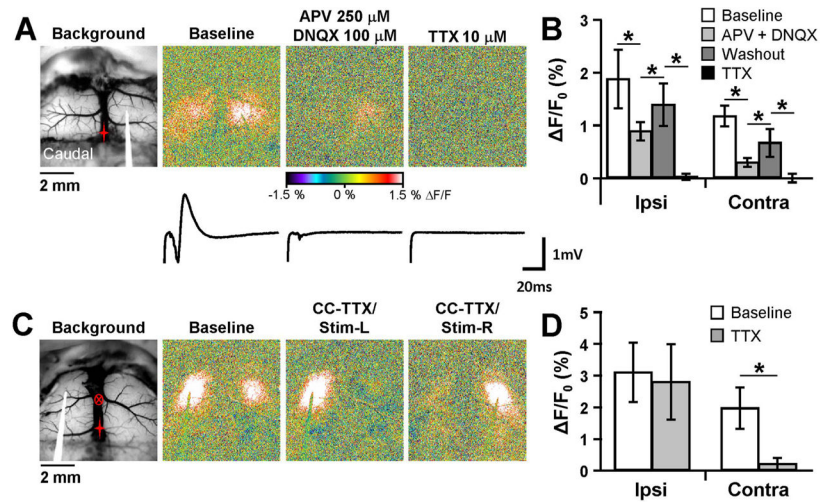
Fig. 2.
Involvement of ionotropic glutamate receptors and the corpus callosum. A. Background and pseudocolored responses to 10 Hz stimulation under baseline conditions (left), or in the presence of either 250 μM APV/100 μM DNQX (middle) or 10 μM TTX (right). Traces below each image correspond to local field potentials in the contralateral hemisphere for the three different conditions. The end of the stimulus artifact is shown at the beginning of each field potential trace. B. Mean peak flavoprotein response from all conditions tested for the ipsilateral and contralateral hemispheres (n=4). C. Flavoprotein response in the same animal before and after TTX microinjection (circled x) into the corpus callosum. Blocking the corpus callosum (CC-TTX) caused a near complete loss of the contralateral response (middle). Moving the stimulating electrode to the other hemisphere in the same animal (right) still resulted in a similar ipsilateral response, but failed to show a contralateral response. D. Population (n=4) showing abolishment of the contralateral response following TTX blockade of the corpus callosum.
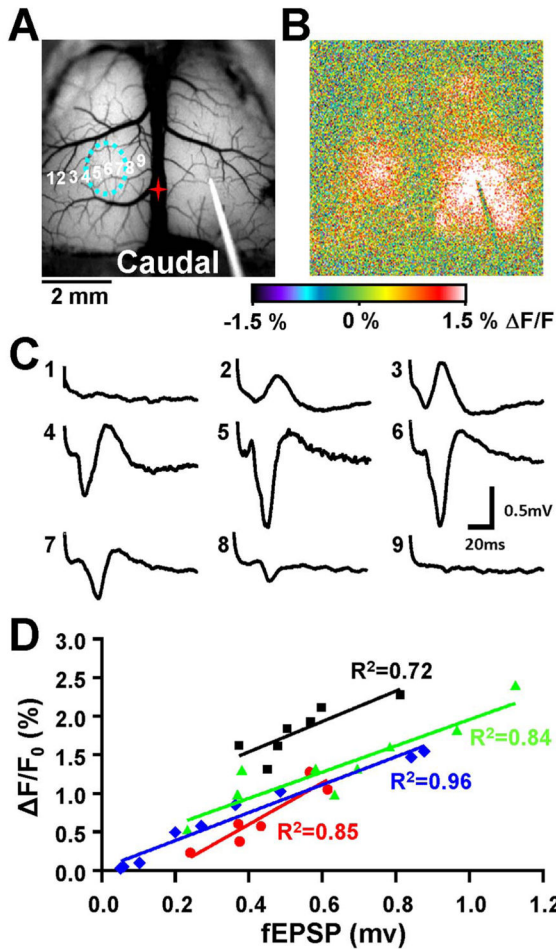
Fig. 3.
Local field potentials correlate with the contralateral flavoprotein response. A. Brightfield image showing placement of the stimulating electrode on the right hemisphere, with several different recording locations (numbered 1–9) on the left hemisphere. The dashed blue circle corresponds to the area of maximal fluorescence increase determined following stimulation. B. Pseudocolored flavoprotein image during the maximal contralateral response. C. Local field potentials at the different recording sites shown in *A* following stimulation. The LFP response increases towards the center of the maximal flavoprotein response (sites 4–6) and decreases farther out on each side. D. Population (n=4, black, green, blue, and red) showing a strong linear relationship between the amplitude of the contralateral flavoprotein response and the amplitude of the LFP response. LFP traces from *C* corresponds to the blue trace.
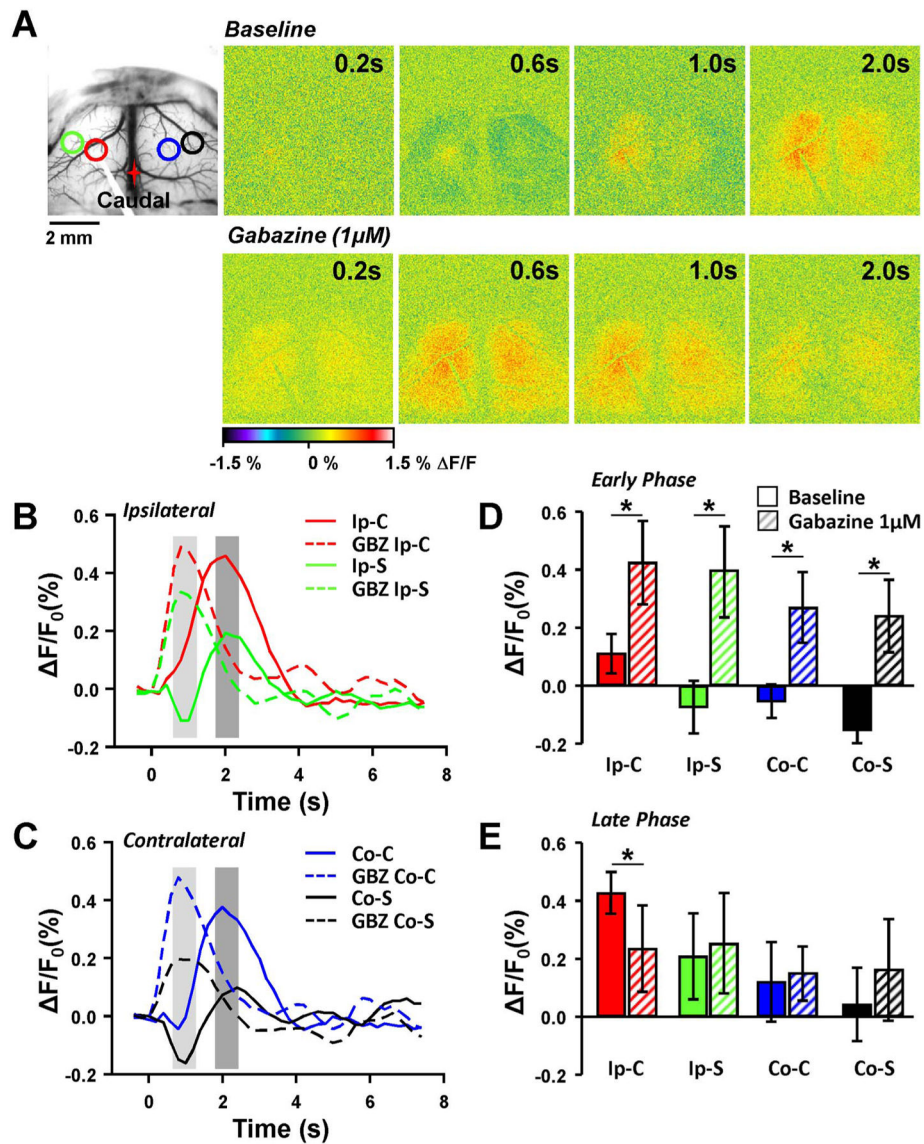
Fig. 4.
Inhibitory response following single pulse stimulation. A. Brightfield image showing placement of stimulating electrode and locations of four different ROIs: Ipsilateral center (Ip-C, red); Ipsilateral surround (Ip-S, green); Contralateral center (Co-C, blue); Contralateral surround (Co-S, black). Pseudocolored flavoprotein response following single pulse stimulation under baseline conditions (top row) and following application of 1 μM Gabazine (GBZ) in the same animal. B. Example flavoprotein traces from the ipsilateral hemisphere following single pulse stimulation in baseline (solid lines) and following GBZ application (dashed lines). The light and dark gray regions indicate two phases of the response that were quantified further, the early and late phase, respectively. C. Same as in *B* except that the responses were collected from the contralateral hemisphere. D. Population data (n=4) from the early phase (light gray regions in *B* and *C*) from baseline (solid bars)

and GBZ treatment (striped bars) from the different ROIs. E. Same as *D* except population data from the late phase.
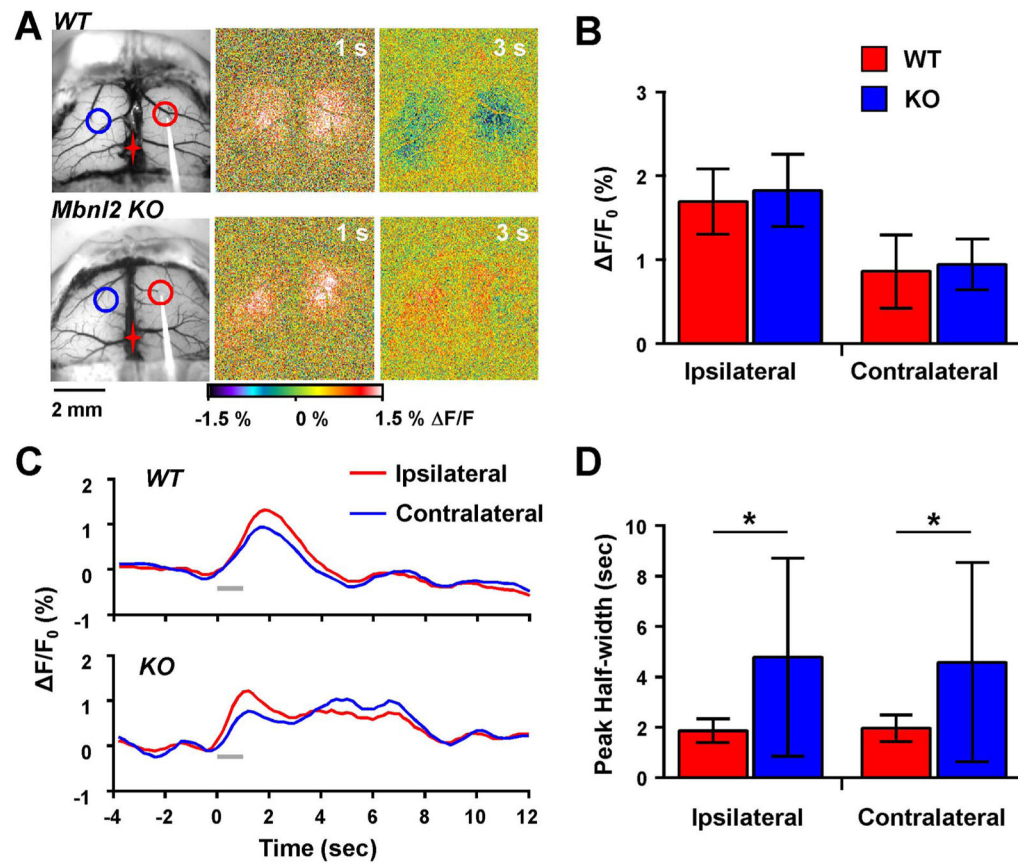
Fig. 5.
Prolonged flavoprotein response in *Mbnl2* KO mice. A. Example images from a WT and
an *Mbnl2* KO mouse following 10 Hz stimulation. A prolonged increase in flavoprotein
signal was observed in the *Mbnl2* KO mouse. Red and blue circles represent ROIs for
the ipsilateral and contralateral hemispheres, respectively. B. Quantification of the peak
flavoprotein response revealed no significant difference between WT (n=7) and MBNL2 KO
mice (n=8). C. Example flavoprotein traces from a WT and *Mbnl2* KO mouse highlight the
prolonged increase in the time course of the flavoprotein response in the *Mbnl2* KO. D.
Mean changes in the duration of the flavoprotein response measured by the peak half-width
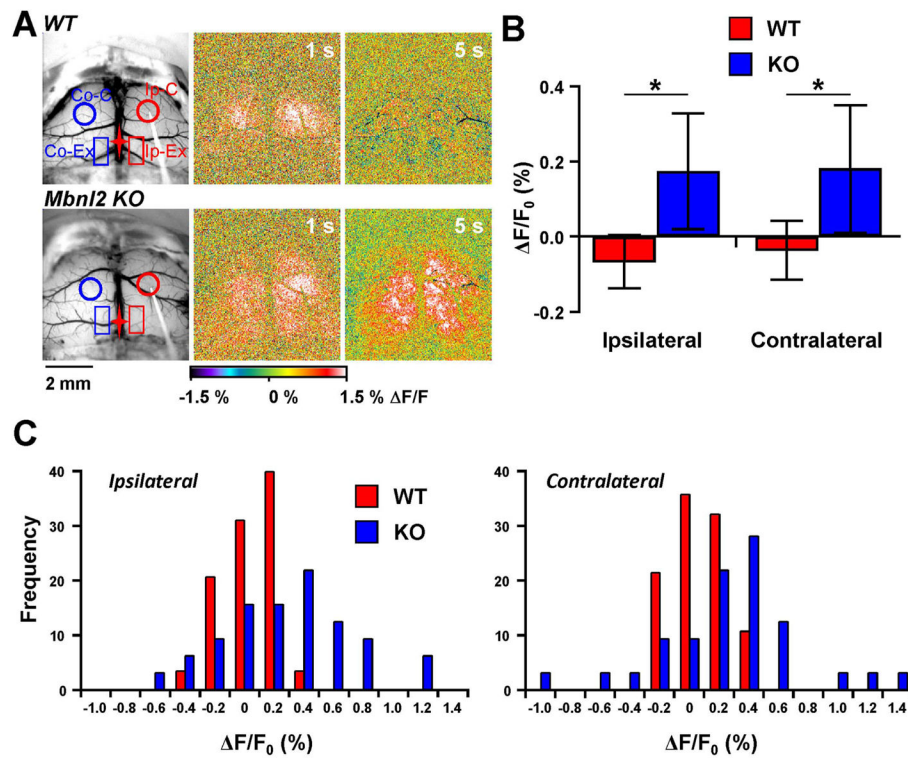show a significant increase in the flavoprotein duration in *Mbnl2* KO mice.

Fig. 6.
Additional regions activated in *Mbnl2* KO mice following 10 Hz stimulation. A. Example images from WT and *Mbnl2* KO mice showing the placement of two new rectangular ROIs: Ip-Ex, ipsilateral extra region; and Co-Ex, contralateral extra region. Pseudocolored images show the larger flavoprotein response area in the *Mbnl2* KO mouse at 5 s compared to the WT mouse. B. Average peak flavoprotein increase in the extra regions show significant increases compared to WT mice (WT=7, KO=8). C. Distributions of the peak flavoprotein response from the extra regions in the ipsilateral and contralateral hemispheres.
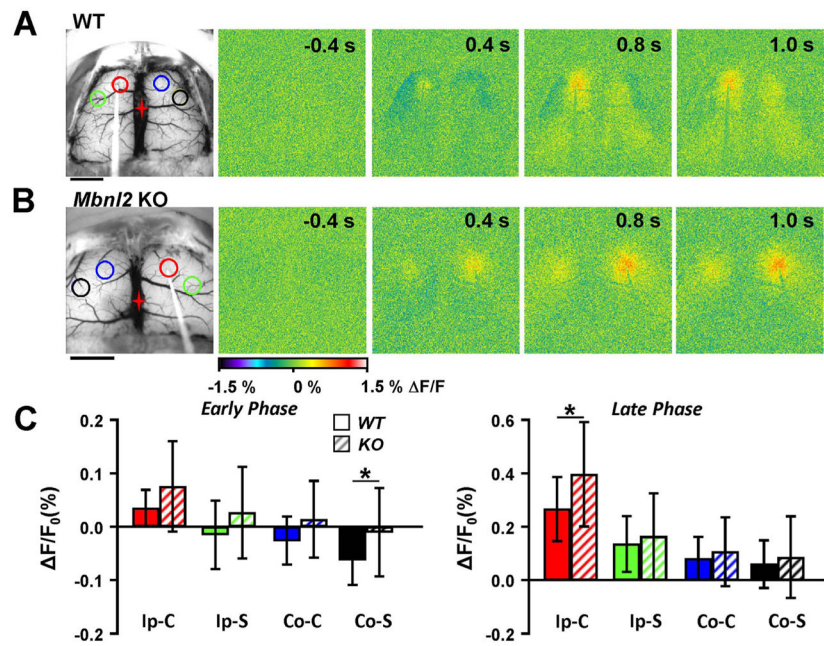
Fig. 7.
Reduced inhibitory-like surround in *Mbnl2* KO mice following single pulse stimulation.
A. Example images from a WT mouse following single pulse stimulation, and location of the ROIs. Scale bar =2 mm. B. Flavoprotein responses from an example *Mbnl2* KO mouse following single pulse stimulation. Scale bar=2 mm. C. Average data of the peak flavoprotein response during the early and late phase (see Fig. 4) in WT (n=7, solid bars) and *Mbnl2* KO mice (n=8, striped bars).
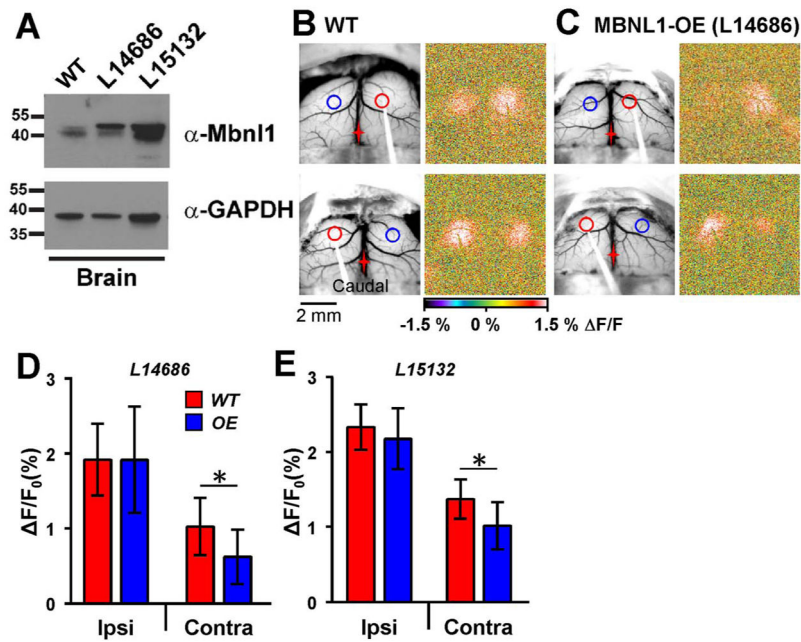
Fig. 8.
Decreased contralateral response in mice over-expressing MBNL1. A. Expression of MBNL1 in transgenic overexpression mouse lines. Western blot analysis of protein extracted from the brain of WT, L14686 (original) and L15132 (newly developed) transgenic mouse lines. Blots were probed with either an antibody against Mbnl1 (A2764, gift from Dr. Charles Thornton, University of Rochester) or GAPDH (Millipore, MAB374). B. Example images from a WT mouse where 10 Hz stimulation was performed on the right (top) and left (bottom) hemispheres. C. Images from an MBNL1-OE mouse (L14686). Responses on the contralateral hemisphere were significantly smaller regardless of which hemisphere was stimulated. D and E. Quantification of the peak flavoprotein responses from two different MBNL1-OE lines: L14686 (*D*, WT=8, OE=8); and L15132 (*E*, WT=6, OE=7). Both MBNL1-OE lines showed a significant decrease in the contralateral response compared to WT mice.
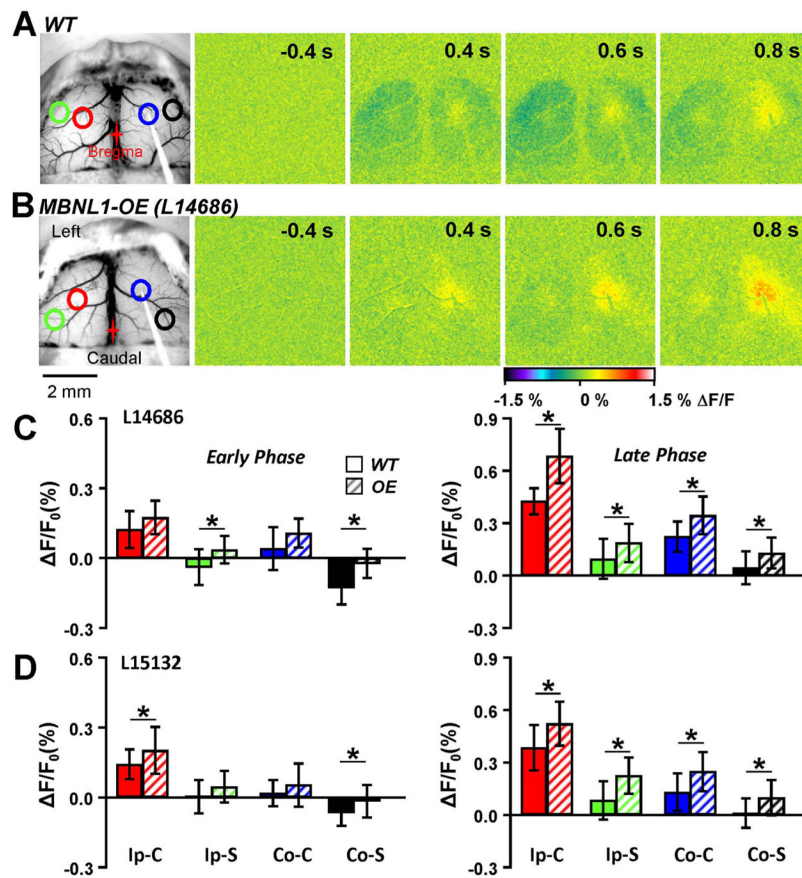
Fig. 9.
Impairment of inhibitory activity following single pulse stimulation in MBNL1-OE mice. A.
Example images from a WT mouse following single pulse stimulation. Similar results were
observed to that in Fig. 4, with a region of decreased flavoprotein fluorescence surrounding
a local increase. B. Responses from an example MBNL1-OE mouse following single pulse
stimulation revealed a near lack of flavoprotein decrease in the ipsilateral and contralateral
surrounding areas. C. Quantification of the peak flavoprotein response in L14686 (WT=6,
OE=5) from the four different ROIs in the early (left) and late (right) phase described in Fig.
4. D. Same as *C* except for L15132 (WT=7, OE=7). Both lines showed a larger fluorescence
response in the surrounding ROIs compared to the WT mice.